Effect of large strain cold rolling and subsequent annealing on microstructure and mechanical properties of an austenitic stainless steel

I. Shakhova , V. Dudko , A. Belyakov , K. Tsuzaki , R. Kaibyshev

Keywords:
Nanostructured materials
Austenite
Large strain cold rolling
Grain refinement
Phase transformation
Recrystallization

A B S T R A C T

The microstructural evolution of an S304H steel during bar rolling to a strain of 4 and subsequent annealing as well as its effect on the mechanical properties were investigated. The cold working was accompanied by a strain-induced martensitic transformation, leading to the development of lamellar-type microstructure consisting of highly elongated austenite/ferrite subgrains with a mean transverse size of approximately 50 nm; the austenite volume fraction was approximately 0.35. This material exhibited a yield strength above 2000 MPa. The subsequent annealing resulted in grain coarsening following the ferrite → austenite reversion, which led to almost full austenitization at temperatures above 700 °C. The formation of the austenite/ferrite lamellar structure that mixed with separate equiaxed grains occurred after annealing at temperatures of $T \leq 700$ °C. The grain coarsening was accompanied by a degradation in strength, although the yield strength of above 1000 MPa remained after 2 h of annealing at 700 °C. The discontinuous recrystallization of austenite resulted in the development of a relatively coarse-grained microstructure at $T \geq 800$ °C.

1. Introduction

Steels and alloys with nanocrystalline and submicrocrystalline structures are considered advanced engineering materials due to the favorable combination of their mechanical properties [1–5]. Among a number of proposed methods for developing nanograined structures in various metallic materials, severe plastic deformation is the most attractive technique enabling the fabrication of commercially sizeable products [6,7]. Special practical interest is aroused by the methods of severe plastic deformation that are based on conventional metal working techniques and can be used for commercial applications. According to recent studies, the total strain is the most important property for the development of nano/submicrocrystalline structures in metallic materials, whereas processing methods do not play a crucial role in the microstructural evolution [8,9]. Therefore, conventional metal-working techniques, in which one or more dimensions of the work piece is continuously reduced under processing, can be used instead of laborious, redundant, shape-change processes if the kinetics of grain refinement are fast enough for the complete evolution of the nano/submicrocrystalline structure at moderate strains.

Various metals and alloys are characterized by remarkably different kinetics of grain refinement during severe deformation [10–13]. The rapid development of nano/submicrocrystalline structures has been observed for materials allowing pronounced grain subdivision upon plastic working. Typical representatives of such materials are metastable austenitic steels [14,15]. The grain refinement in these materials is accelerated by multiple mechanical twinning and/or strain-induced phase transformation, leading to the fast development of nano/submicrocrystalline structures at relatively small strains, which can be easily attained by ordinary cold rolling. Both the twinning and the martensitic transformation depend on the stacking fault energy (SFE). Twinning has been reported to occur in steels with an SFE above 12–18 mJ m^{-2}, while the formation of martensite requires an SFE below approximately 18 mJ m^{-2} [16–19]. Therefore, austenitic stainless steels with a relatively low SFE can be processed in high-strength products by means of extensive grain refinement. The yield strength can be drastically increased from 250–350 MPa to 1200–1600 MPa by using a thermomechanical treatment consisting of cold rolling with a total reduction ranging from 50 to 90%, which generates the strain-induced martensite, followed by the phase reversion during a final annealing step [14,20–23].

The formation of ultrafine-grained structure in Cr–Ni austenitic stainless steels by the reversion from deformation-induced martensite has been studied in a number of recent studies [14,16,24–32]. The cold rolling brings about a high dislocation density along with dense deformation twins with nanoscale

spacing. Then, the deformation-induced martensite nucleates at shear bands and deformation twins [16,31,32]. Because the austenitic stainless steels are thermodynamically metastable at room temperature, the austenite easily transforms into deformation-induced martensite with increasing strain [14,24–31,33]. Upon subsequent annealing, the martensite transforms to austenite by shear reversion and/or diffusional (nucleation and growth) reversion mechanisms [14,25,28,33]. The following set of criteria for ultra grain refinement by reversion from deformation-induced martensite was reported by Tomimura et al. [24]: (i) austenite should be almost completely transformed to martensite during cold rolling; (ii) most of the martensite must revert to austenite at a relatively low temperature to avoid grain growth in the reversed austenite; and (iii) the martensite start temperature of the reversed austenite should be below room temperature. The range of C, Ni and Cr compositions of austenitic stainless steels that meet these criteria was considered as well [24].

Recently, an S304H austenitic stainless steel was developed for high-temperature applications [34]. This steel exhibits increased strength and creep resistance with respect to conventional AISI 304 steel, which is associated with dispersion strengthening mainly by Nb(C, N) precipitation. It is expected that this steel, which exhibits nano/submicrocrystalline structure, can exhibit superior strength properties. The value of the SFE in 304-type stainless steels has been reported to be approximately 20 mJ m^{-2} [35,36]. Hence, the mechanical twinning and martensitic transformation are expected to occur concurrently during cold working. The aim of the present work is to explore the feasibility of producing nano/submicrocrystalline structures in an S304H steel by large-strain cold rolling and subsequent annealing. The regularities of microstructural evolution during deformation and annealing were examined in detail to address the relationship between the developed microstructures and the observed mechanical properties.

2. Experimental procedure

An S304H austenitic stainless steel, Fe–0.1C–0.12N–0.1Si –0.95Mn–18.4Cr–7.85Ni–2.24Cu–0.5Nb–0.01P–0.006S (all in mass%), was used as starting material. The steel was hot rolled and then annealed at 1100 °C for 10 min. The mean grain size was 10 ± 1 μm. The cold working was carried out by caliber rolling 9.2 mm × 9.2 mm square bars into 1.25 mm × 1.25 mm square bars at ambient temperature, leading to a total strain of 4. The cold worked rods were cut into specimens of 70-mm in length and annealed in a muffle furnace at temperatures ranging from 400 to 900 °C followed by water quenching.

Strain hardening and annealing softening were studied using Vickers microhardness tests with a load of 1 N. The mechanical properties were evaluated using tensile tests. The specimens with an 8-mm gauge length were prepared by an electric-discharge method. The tensile axis was parallel to the rolling axis. The mechanical tests that were conducted on samples rolled to a strain of 4 and then annealed at different temperatures were performed at ambient temperature using an Instron 5882 testing machine.

Structural investigations were performed on sections parallel to the rolling axis using a JEM-2100 transmission electron microscope (TEM) and a Quanta 600 FEG scanning electron microscope equipped with an electron back-scattering diffraction (EBSD) analyzer incorporating an orientation imaging microscopy system. In addition to EBSD, the phase content, i.e., austenite/ferrite fraction, was evaluated by magnetic force microscopy (MFM) using an NTEGRA Aura scanning probe microscope. The grain/subgrain sizes were measured perpendicular to the rolling axis by a linear-intercept method used to count all boundaries, including dislocation sub-boundaries revealed by TEM micrographs. The dislocation densities were estimated by counting individual dislocations in grain/subgrain interiors in at least six arbitrarily selected TEM images for each data point [37]. Misorientations between nanocrystallites were analyzed by the conventional TEM Kikuchi-line method using the converged-beam technique [38]. Equilibrium volume fractions of the austenite at various temperatures were calculated with the software program ThermoCalc using a TCFE6 database (300 K was used as the ambient temperature).

3. Results

3.1. Strain hardening and structural changes during cold working

The cold rolling of an S304H austenitic stainless steel results in significant hardening (Fig. 1). The most pronounced strain hardening occurs at relatively small strains. The cold rolling to a strain of 0.4 is accompanied by a twofold increase in hardness from 1695 MPa in the initial annealed state to 3275 MPa. Then, the rate of strain hardening decreases to a value of approximately 700 MPa per strain, which remains almost constant during further processing. As a result, the hardness increases almost linearly with an increasing total strain from 0.4 to 4.0. Such deformation behavior is not typical of fcc metallic materials subjected to large-strain cold working. Commonly, the rate of strain hardening gradually decreases during deformation, ultimately approaching nearly zero after sufficiently large strains are sustained [39–42]. The continuous increase in the hardness is indicative of ongoing structural strengthening.

Typical deformation microstructures that developed in an austenitic stainless steel during caliber cold rolling are shown in Fig. 2. Early deformation leads to the elongation of original grains along the direction of plastic flow and results in the development of various strain-induced boundaries, most of which are associated with deformation twinning (Fig. 2a). The number of twins increases with straining (Fig. 2b). Because the austenite in the studied steel is metastable at room temperature, a partial martensitic transformation occurs during cold rolling to strains above 1. The twinning and the martensitic transformation promote grain refinement, leading to the development of dual-phase structures consisting of austenite and ferrite grains. The former can be roughly distinguished as being red and blue (⟨1 0 0⟩ and ⟨1 1 1⟩ parallel to the rolling axis) and the latter as being green (⟨1 1 0⟩ parallel to the rolling axis) in Fig. 2c and d.

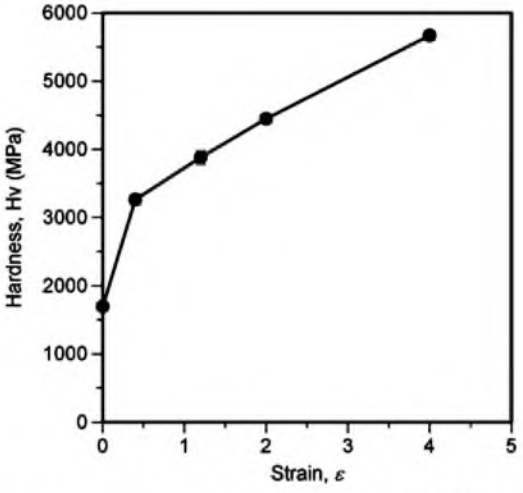

Fig. 1. Strain hardening of an S304H austenitic stainless steel subjected to large-strain cold rolling.

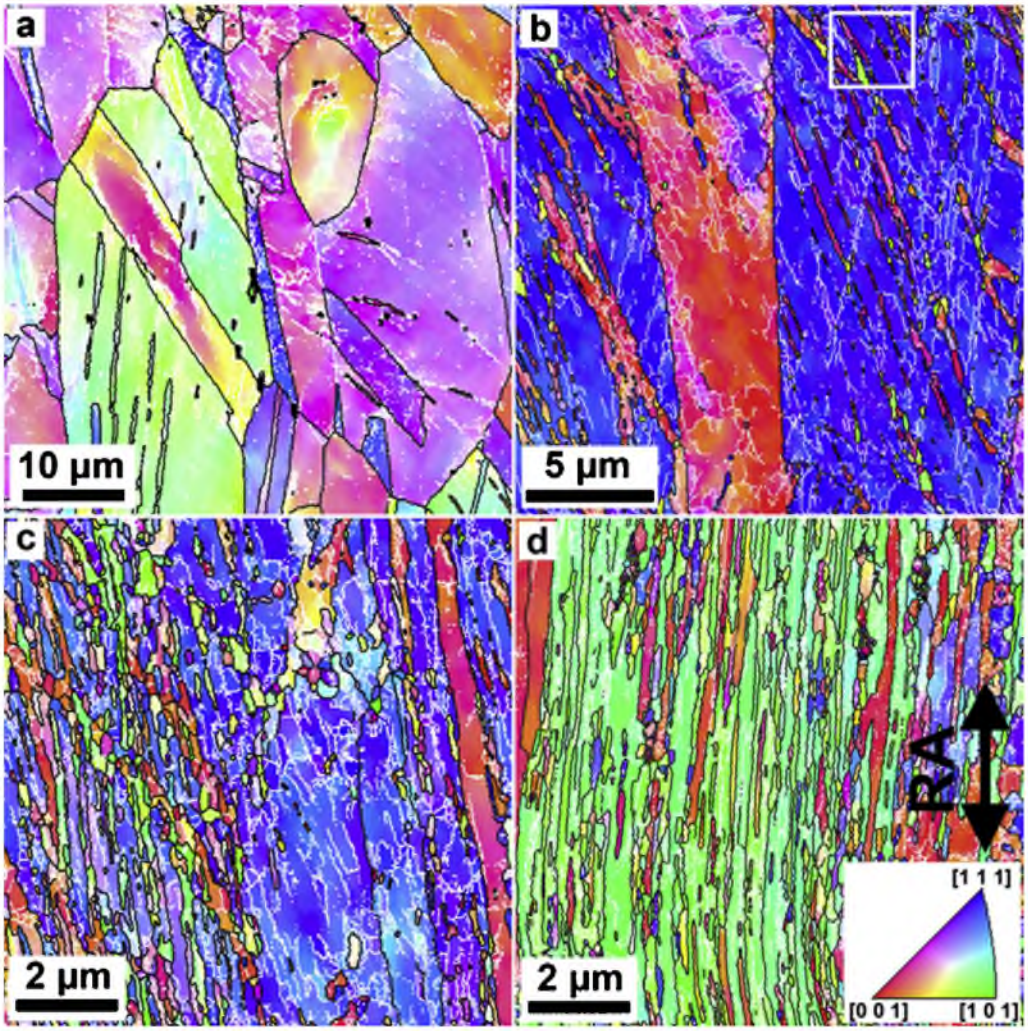

Fig. 2. Typical microstructures in an S304H austenitic stainless steel subjected to cold rolling to a total strain of 0.4 (a), 1.2 (b), 2 (c) and 4 (d). The white and black lines indicate the low- and high-angle boundaries, respectively. The inverse pole figures are shown for the rolling axis (RA). (For interpretation of the references to color in this figure legend, the reader is referred to the web version of the article.)

Let us consider the structural changes during the cold rolling in more detail. Cold rolling to a relatively small strain of 0.4 promotes the evolution of high dislocation density and the development of lamellar subgrains within the initial grains (Fig. 3). Two types of lamellae can be distinguished. The first component of the lamellar structures is the deformation microbands outlined by strain-induced sub-boundaries. The second component involves two families of deformation twins. These types of deformation substructure consisting of high dislocation density and deformation twins with different {1 1 1} twin planes were frequently observed in austenitic stainless steels subjected to cold working to relatively small strains [31,43,44].

Upon further straining to 1.2, the density of twins increases greatly; numerous strain-induced boundaries of austenite lamellas having low- to high-angle misorientations evolve (Fig. 4), a process similar to continuous dynamic recrystallization [10,40,42,45–48]. Closely spaced twins and deformation-induced boundaries comprise the clusters that appear as shear bands at the meso-scale level. Rolling to strains above 1 initiates the martensitic transformation. The martensite starts to develop primarily at deformation twins (Fig. 5). Several orientation relationships have been proposed for the austenite–ferrite transformation [33,49,50]: the Kurdjumov–Sachs (K–S), $(1\,1\,1)_\gamma||(0\,1\,1)_\alpha$, $[-1\,0\,1]_\gamma||[-1\,-1\,1]_\alpha$; the Nishiyama–Wasserman (N–W), $(1\,1\,1)_\gamma||(0\,1\,1)_\alpha$, $[1\,0\,-2]_\gamma||[0\,-1\,1]_\alpha$; the Pitsch (P), $(1\,0\,0)_\gamma||(0\,-1\,1)_\alpha$, $[0\,-1\,-1]_\gamma||[1\,-1\,-1]_\alpha$; the Greninger–Troiano (G–T), $(1\,1\,1)_\gamma||(0\,1\,1)_\alpha$, $[-12\,-5\,17]_\gamma||[-7\,17\,-17]_\alpha$; and the inverse Greninger–Troiano (G–T′), $(0\,1\,1)_\gamma||(1\,1\,1)_\alpha$, $[7\,-17\,17]_\gamma||[-5\,-12\,17]_\alpha$. It should be noted that all of these orientation relationships can be described by close values of rotation angles (θ) and axes $\langle UVW\rangle$ (Table 1). The measured rotation angles between the selected austenite and martensite grains do not exactly match any of the predicted relationships (Table 1). The deviations from predicted orientations are equal to 4–5°, although the orientation of the martensite grain indicated by the letter F is quite close to the Greninger–Troiano and/or Pitsch relationships.

At a strain of 2, a well-defined lamellar structure developed (Fig. 6a). It should be noted that mechanical twinning continues to be operative within austenitic grains even at large strains. The subdivision of some grains by twins with an average spacing between neighboring twin boundaries of 10 nm leads to the formation of nano-twinned structure (Fig. 6b). Additionally, the progressive formation of deformation martensite leads to the substitution of austenite lamellae by ferrite lamellae. The lamellar-type structure composed of alternating nano-scale austenite and ferrite grains is evolved at a strain of 4 (Fig. 7). The both austenite and ferrite grains are highly elongated along the rolling axis; their transverse sizes of

Table 1
Orientation relationships between austenite and martensite grains in a sample strained to 1.2 (see lettered portions in Fig. 5).

Rotation	Rotation angle and axis, θ $\langle UVW \rangle$	Deviation from predicted orientations				
		ΔK–S	ΔN–W	ΔP	ΔG–T	ΔG–T′
K–S	42.9° ⟨0.178; −0.178; 0.968⟩	0°	5.3°	5.3°	2.4°	2.4°
N–W	46.0° ⟨0.201; −0.083; 0.976⟩	5.3°	0°	7.4°	2.9°	5.8°
P	46.0° ⟨−0.201; −0.083; 0.976⟩	5.3°	7.4°	0°	5.8°	2.9°
G–T	44.2° ⟨0.189; −0.133; 0.973⟩	2.4°	2.9°	5.8°	0°	3.4°
G–T′	44.2° ⟨−0.189; −0.133; 0.973⟩	2.4°	5.8°	2.9°	3.4°	0°
A, C	46.0° ⟨−0.154; −0.273; 0.950⟩	5.4°	4.7°	8.8°	4.3°	6.7°
B, C	44.7° ⟨0.109; 0.991; −0.073⟩	5.8°	5.9°	4.4°	5.2°	4.5°
D, F	45.2° ⟨0.054; 0.158; −0.986⟩	5.7°	6.4°	2.5°	5.4°	3.7°
E, F	45.1° ⟨0.963; −0.153; −0.221⟩	3.1°	3.4°	6.5°	1.9°	4.2°
H, G	39.9° ⟨0.142; −0.133; −0.981⟩	3.8°	7.2°	6.9°	4.9°	4.8°

approximately 50 nm are almost the same. The longitudinal boundaries are characterized by random misorientations ranging from small angles typical for dislocation sub-boundaries to large angles inherent to ordinary grain boundaries (Fig. 7b).

Fig. 8 summarizes the effect of strain on the austenite fraction, the transverse grain/subgrain size and the dislocation density in subgrain interiors. A significant change in the austenite fraction due to martensitic transformation occurs during the deformation to a strain of 2, when the fraction of deformation martensite increases to 0.5. Then, the transformation kinetics slows down. The austenite fraction decreases to approximately 0.35 after rolling to a total strain of 4, which is more than twice as large as the austenite fraction of 0.16 predicted by ThermoCalc (Fig. 8). This finding suggests that Cu addition decreases the rate of martensitic transformation under cold working relative to that of 304 stainless steel, in which the austenite was almost fully transformed at strain of 1 [30]. Nevertheless, the structural refinement is characterized by very fast kinetics in the strain range of 0 to 1. The transverse grain/subgrain size rapidly reduces to approximately 50 nm after rolling to a total strain of 1.2, whereas further processing is not accompanied by a

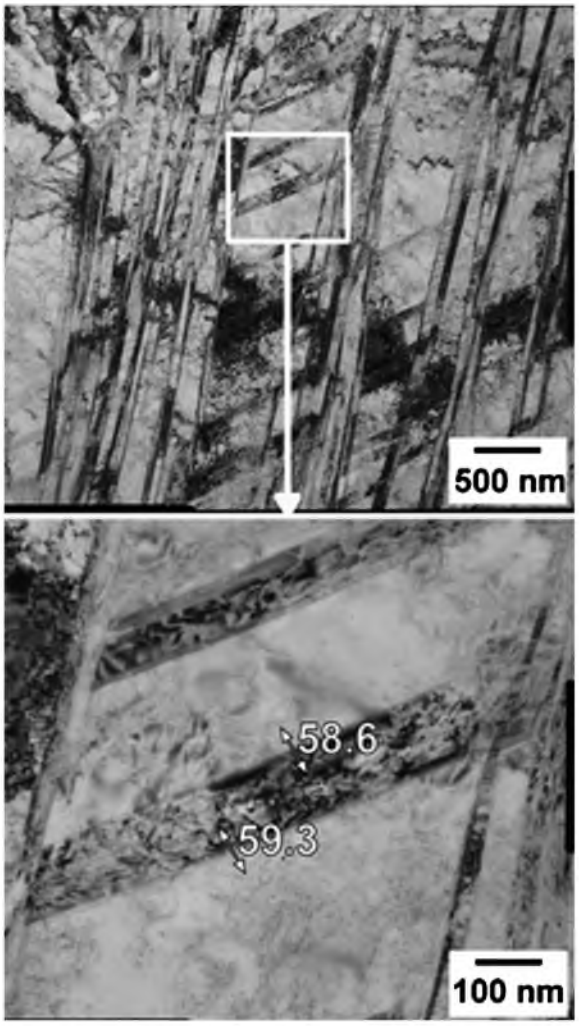

Fig. 3. Typical sub-structures developed in an S304H austenitic stainless steel after cold rolling to a strain of 0.4. The numbers indicate the grain boundary misorientations in degrees.

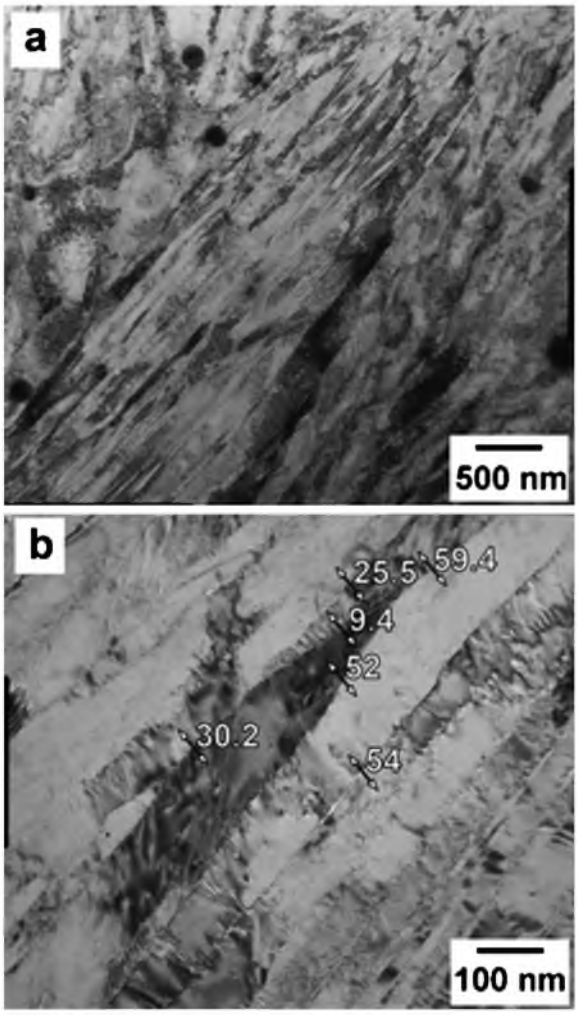

Fig. 4. Typical sub-structures developed in an S304H austenitic stainless steel after cold rolling to a strain of 1.2. The numbers indicate the sub-boundary misorientations in degrees.

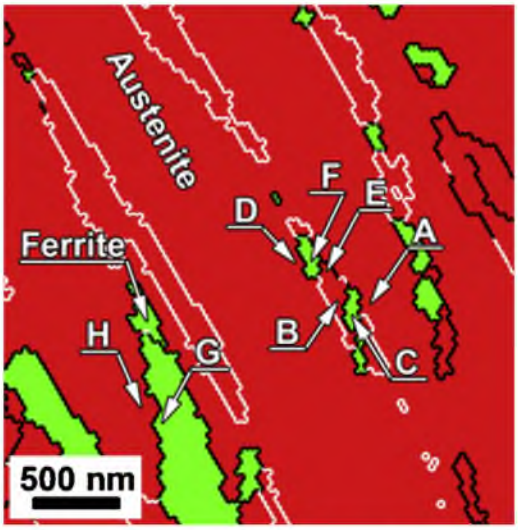

Fig. 5. Enlarged image of the selected portion in Fig. 2b that shows the appearance of ferrite (deformation-induced martensite) in a sample strained to 1.2. The white and black lines indicate CSL with Σ3 and ordinary high-angle boundaries, respectively.

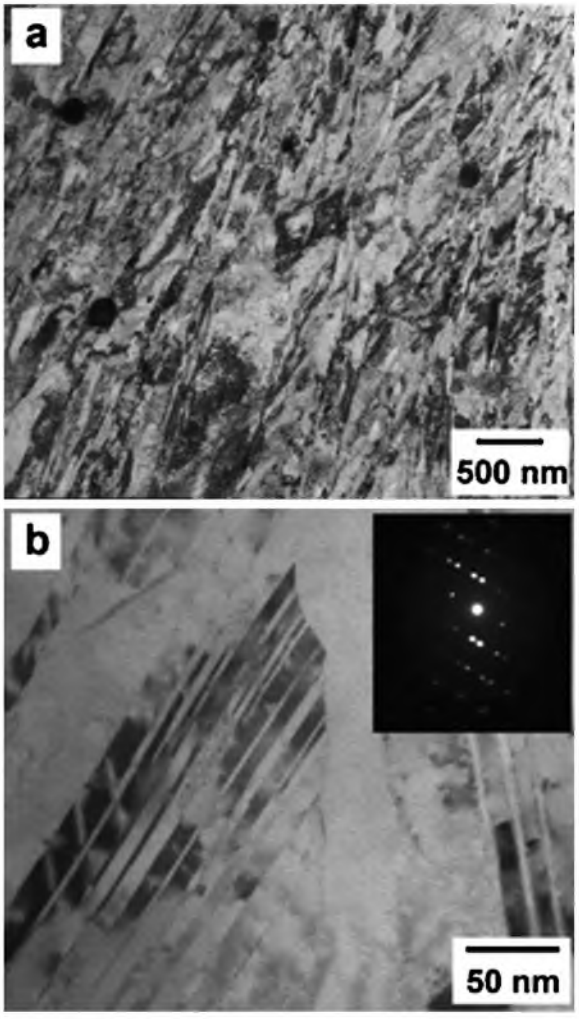

Fig. 6. TEM micrographs of layered sub-structure (a) and deformation twins (b) developed in an S304H austenitic stainless steel after cold rolling to a strain of 2.

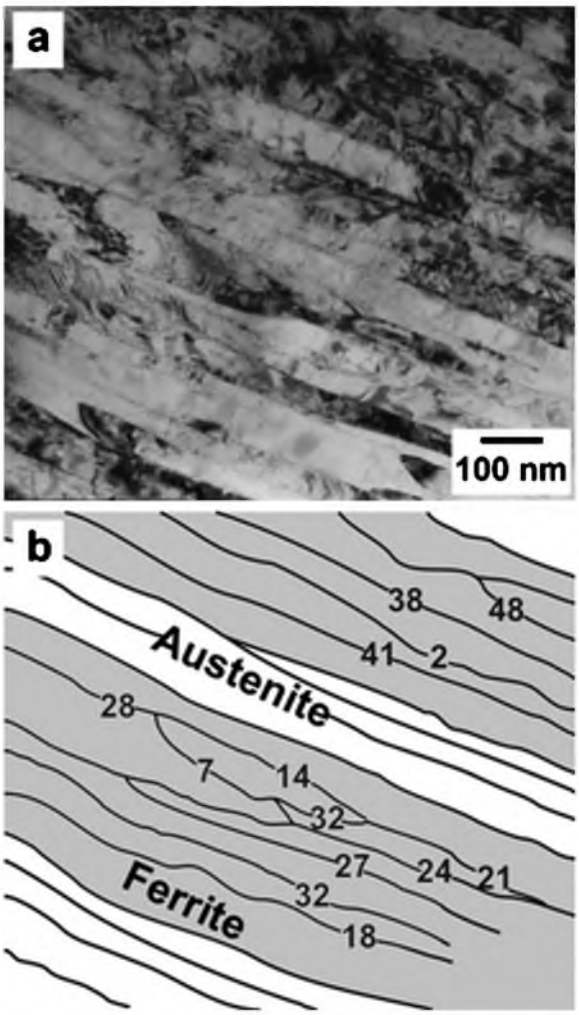

Fig. 7. Typical sub-structures developed in an S304H austenitic stainless steel after cold rolling to a strain of 4. Numbers indicate the sub-boundary misorientations in degrees.

remarkable change in the transverse size of structural elements. The rapid structural refinement at an early deformation is accompanied by the increase in the dislocation density, which reaches $1.5 \times 10^{15}\ m^{-2}$ after straining to 0.4. The martensitic transformation during subsequent cold rolling leads to a further increase in the dislocation density, approaching $4 \times 10^{15}\ m^{-2}$ at a total strain of 2. It is interesting that the cold rolling to larger strains is accompanied by an apparent decrease in the density of lattice dislocations in grain/subgrain interiors. A similar tendency was observed in other studies on large strain deformation [7,9,10,40]. Evidently, the closely spaced lamellar boundaries act as dislocation sinks. The lattice dislocations move across lamellae and can be easily trapped by the boundaries.

3.2. Annealing behavior

Annealing at temperatures below 800 °C does not lead to remarkable structural coarsening (Fig. 9). The microstructure evolution during annealing is mainly associated with the development of new fine austenite grains. Some of the new grains exhibit an almost equiaxed shape that changes the lamellar morphology of the deformation microstructure developed by cold rolling. The formation of new fine grains results from the inverse phase transformation. The austenite fraction is approximately 0.65 and 0.9 after annealing at 600 °C and 700 °C, respectively. The high

Table 2
Orientation relationships between austenite and ferrite grains in a sample strained to 4 and then annealed at 600 °C for 30 min (see lettered portions in Fig. 10).

Rotation	Rotation angle and axis, θ ⟨UVW⟩	Deviation from predicted orientations				
		ΔK–S	ΔN–W	ΔP	ΔG–T	ΔG–T′
F, A	38.2° ⟨0.874; −0.004; −0.486⟩	15.2°	15.0°	15.1°	14.9°	15.0°
F, G	35.2° ⟨0.702; −0.107; −0.704⟩	23.8°	25.1°	25.0°	24.3°	24.2°
E, B	36.7° ⟨0.135; −0.449; 0.883⟩	12.5°	16.3°	13.8°	14.9°	12.8°
C, D	44.1° ⟨0.989; −0.12; 0.088⟩	4.8°	4.1°	5.5°	3.6°	4.4°
H, I	39.3° ⟨−0.127; 0.954; −0.271⟩	5.6°	10.8°	7.5°	7.9°	6.0°
K, J	45.5° ⟨−0.053; −0.235; 0.971⟩	4.7°	2.1°	6.2°	2.6°	4.8°
L, K	41.1° ⟨−0.005; −0.968; −0.250⟩	7.9°	6.3°	6.5°	6.7°	7.0°

nucleation rate in the severely strained samples promotes the simultaneous formation of a great number of new austenite grains upon subsequent heating. Thus, the transverse grain size remains at the submicron level. The mean spacing of high-angle boundaries is approximately 120 nm and 230 nm after annealing at 600 °C and 700 °C, respectively (Fig. 9a and b). The austenite fraction increases to approximately 1.0 with an increase in annealing temperature to 800 °C. Following the phase transformation at temperatures of $T \geq 800$ °C, discontinuous static recrystallization develops (Fig. 9c), which is very similar to the primary recrystallization that occurs upon heating ordinary cold worked metals and alloys. However, the large density of recrystallizing nuclei in the severely deformed steel promotes the development of ultrafine-grained microstructure with a grain size of approximately 2 μm, even after annealing at a rather high temperature of 900 °C (Fig. 9d).

To study the mechanism of ferrite–austenite reversion during annealing, the rotations between some adjacent austenite–ferrite grains were analyzed. The grains selected for the analysis are lettered in Fig. 10, which is a magnified area of Fig. 9a. The rotation angle and axis are listed in Table 2 along with the deviations from the predicted orientation relationships. The rotations of austenite grains indicated by C and K from neighbouring ferrite grains agree closely with G–T and N–W orientation relationships, respectively; the deviations are 2–3°. However, the rotations of other analyzed grains are characterized by rather large deviations from the predicted low-index parallelism conditions. Generally, the mechanisms of shear reversion and diffusion reversion may take place under the studied conditions. The highly elongated austenite grains should be transformed by the shear reversion mechanism, whereas diffusionally reversed austenite grains are expected to be equiaxed. Therefore, the presence of almost equiaxed austenite grains without any low-index parallelism with respect to adjacent ferrite suggests that both the shear and diffusion reversion mechanisms operate concurrently.

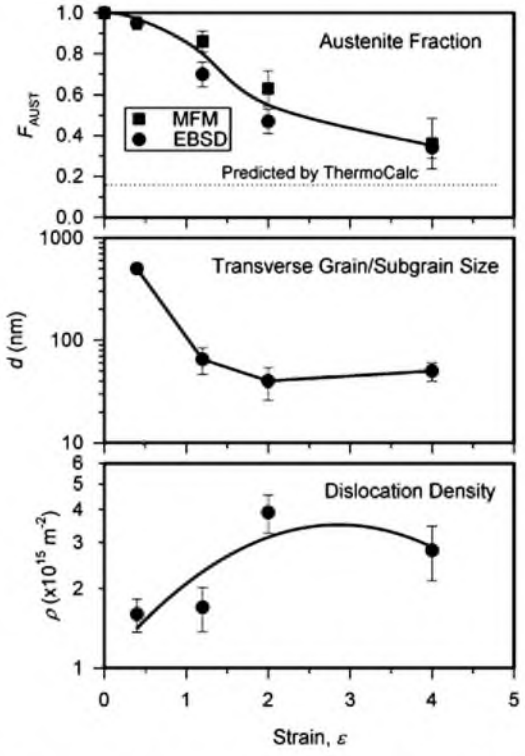

Fig. 8. Effect of cold rolling on the austenite fraction (F_{AUST}), the transverse grain/subgrain size (d) and the dislocation density (ρ) in an S304H austenitic stainless steel.

The dual-phase microstructure consisting of ultrafine austenite and ferrite grains that develops upon the heating of severely deformed steel is rather stable against coarsening over long annealing times. Fig. 11 shows the microstructures evolved by annealing at 600 °C for 2 or 8 h. The mean transverse grain/subgrain size of 90 nm evolved after 30 min of annealing slightly increased to approximately 100 nm after increasing the annealing time to 8 h. Fig. 10 clearly shows that the annealed microstructures consist of a uniform mixture of austenite and ferrite grains with high-angle boundaries. The rapid phase transformation that occurs early during the annealing process results in the development of stable microstructure.

Fig. 12 shows the effect of annealing temperature on the hardness and some structural parameters. Annealing softening is clearly correlated with the structural changes. Two temperature intervals with a separation point at approximately 500 °C can be distinguished. The hardness and the microstructural parameters remain almost unchanged during annealing at $T \leq 500$ °C. On the other hand, annealing at higher temperatures results in gradual softening. The hardness continuously decreases from 5550 MPa to 2610 MPa upon increasing the temperature from 500 °C to 900 °C. The annealing at 900 °C does not fully soften the sample. The hardness of sample treated at this temperature is still higher than that of the original one by almost 1000 MPa. The softening at 500–800 °C is accompanied by a gradual increase in the annealed grain/subgrain size and a decrease in the dislocation density. It should be noted

Table 3
The transverse grain/subgrain size and the mechanical properties of an S304H – type austenitic stainless steel cold rolled to a total strain of 4 and then annealed under various conditions.

Sample	d_{trans} (nm)	Hv (MPa)	$\sigma_{0.2}$ (MPa)	UTS (MPa)	δ (%)
As-processed	50 ± 6	5700 ± 70	2050	2065	2.2
500 °C, 30 min	60 ± 7	5500 ± 30	2090	2180	1.1
500 °C, 2 h	60 ± 7	5710 ± 40	1690	1825	2.0
500 °C, 8 h	70 ± 8	5400 ± 30	1780	1920	2.1
600 °C, 30 min	90 ± 10	4500 ± 70	1410	1475	1.8
600 °C, 2 h	90 ± 10	4970 ± 80	1345	1520	4.7
600 °C, 8 h	100 ± 12	4010 ± 80	1335	1550	5.9
700 °C, 30 min	140 ± 15	3800 ± 40	1145	1225	1.8
700 °C, 2 h	170 ± 20	3680 ± 50	1050	1160	9.0
800 °C, 30 min	450 ± 55	3100 ± 90	670	940	21.1

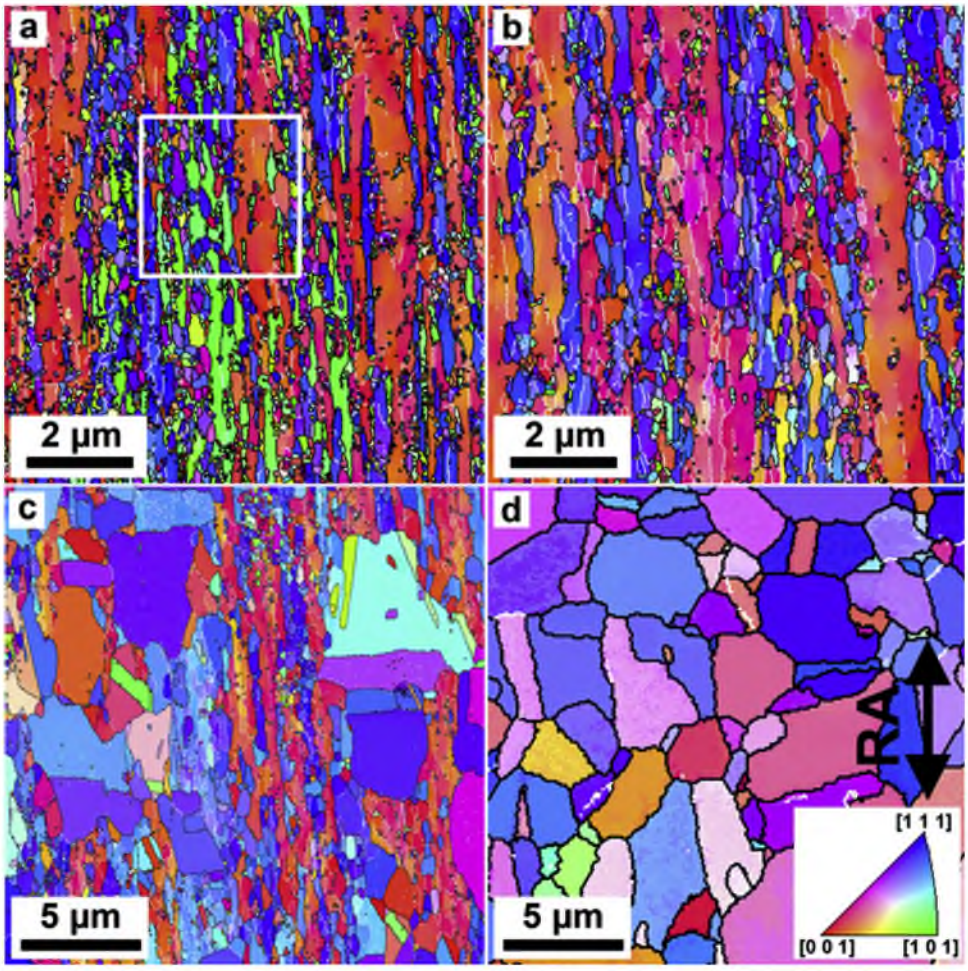

Fig. 9. Typical microstructures in an S304H austenitic stainless steel subjected to cold rolling to a total strain of 4 and then annealed for 30 min at temperatures of 600 °C (a), 700 °C (b), 800 °C (c) and 900 °C (d). The white and black lines indicate the low- and high-angle boundaries, respectively. The inverse pole figures are shown for the rolling axis (RA).

that annealing at temperatures above 500 °C leads to the $\alpha \rightarrow \gamma$ phase transformation. The measured increase in the austenite fraction at temperatures of 500–700 °C is somewhat greater than that predicted by ThermoCalc (dotted line in Fig. 12), which may be associated with the high stored energy in severely strained ferrite.

3.3. *Mechanical properties*

The engineering σ–ε curves are shown in Fig. 13. The steel exhibits a high tensile strength above 2000 MPa in the cold-rolled condition. The tensile behavior is characterized by a well-defined peak in the flow stress and a very short uniform elongation. Namely, after reaching a maximum at a very small strain, the flow stress sharply decreases until fracture. An increase in the temperature gradually reduces the tensile strength. The yield strength decreases to 1780 MPa after annealing at 500 °C for 2 h, while the total elongation remains at a level of approximately 2%, similar to that of cold-rolled condition. The decrease in the flow stresses after annealing at temperatures of $T \geq 600$ °C is accompanied by an increase in the strain, corresponding to a peak stress that leads to a remarkable improvement in ductility. After annealing at 700 °C, an apparent steady state is attained, which provides a significant increase in the uniform elongation. Such an increase in the ductility takes place concurrently with degrading strength, which decreases by approximately two times. Gradual strain hardening through a wide strain range occurs in a specimen annealed at 800 °C, which is

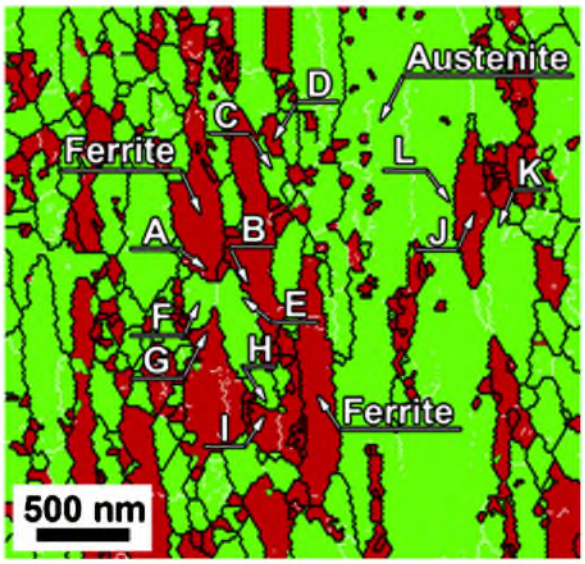

Fig. 10. Enlarged image of the selected portion in Fig. 9a that shows the austenite–ferrite microstructure in a sample strained to 4 and then annealed at 600 °C for 30 min. The white and black lines indicate the low- and high-angle boundaries, respectively.

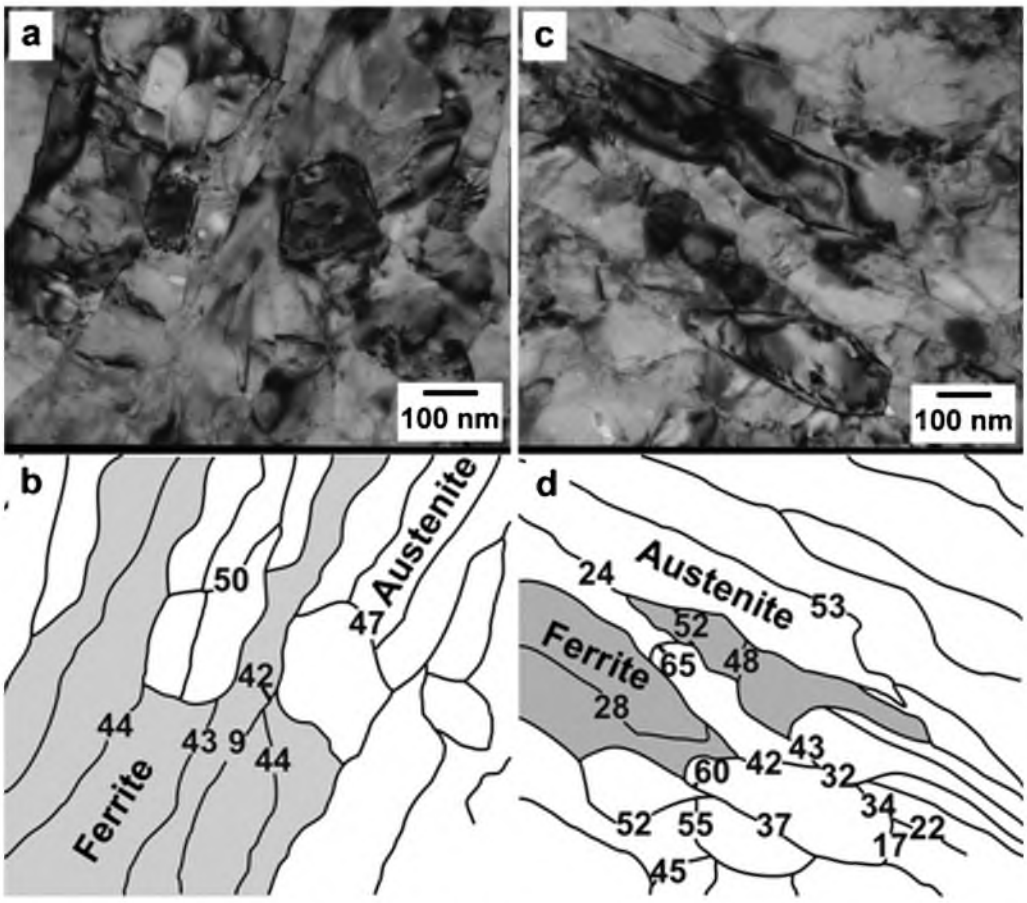

Fig. 11. Typical annealed microstructures with corresponding schematic drawings of sub-boundary distributions developed in an S304H austenitic stainless steel after cold rolling to a total strain of 4 and then annealed at 600 °C for 2 h (a, b) and 8 h (c, d). The numbers indicate the sub-boundary misorientations in degrees. The austenite and ferrite grains are shown in white and grey in (b) and (d).

similar to the tensile behavior of conventional recrystallized materials.

The effects of annealing temperature on the mean grain/subgrain size and the mechanical properties of the cold-rolled and annealed samples are summarized in Table 3. The strength levels in the samples annealed at 500–700 °C depend mainly on the temperature, whereas the annealing time has a minor effect on the mechanical properties. This finding is attributed to the structural stability. The static recovery at relatively low temperature of 500 °C does not lead to significant structural changes in the severely deformed samples, irrespective of the annealing time. At higher temperatures of 600–700 °C, the structural stability over long holding times is provided by the duplex microstructure consisting of austenite and ferrite grains, which are uniformly distributed throughout the specimens.

4. Discussion

The sequence of structural changes leading to the development of nano/submicrocrystalline structures in an S304H stainless steel subjected to large-strain cold rolling and subsequent annealing is schematically represented in Fig. 14. The increasing dislocation density observed early during deformation promotes deformation twinning. The twinning and the formation of deformation microbands provide strain hardening in the strain range of 0.4–1. In turn, the formation of multiply twinned structures is a pre-requisite condition for the initiation of martensitic transformation [31]. In the strain interval of 1–2, the martensitic transformation plays a major role in strengthening due to the development of lamellar structures with high dislocation densities. Upon further straining, the formation of lamellar structures with an average spacing between subgrain boundaries of less than 1 μm greatly increases the critical shear stress required for twinning [51]. Because the twins serve as nucleation sites for the deformation martensite [31], their disappearance slows down the martensitic transformation. Therefore, the martensite (ferrite) volume fraction tends to saturate at a level that is well above the value predicted by ThermoCalc. The boundaries of thin lamellae are effective trapping sites for mobile dislocations. The interaction of the trapped dislocations with twin boundaries and low-angle deformation sub-boundaries results in the gradual evolution of high-angle grain boundaries, which are characterized by a large density of extrinsic dislocations [52]. The development of nanocrystallites with non-equilibrium boundaries is responsible for strain hardening at large strains.

The mechanisms of microstructural evolution during the annealing of severely strained steel consist of ferrite–austenite reversion and the recrystallization of austenite. The phase transformation includes a shear-type reversion and a diffusion-type reversion. At 600–700 °C, both reversion types take place. The appearance of equiaxed austenite grains suggests diffusion reversion, while the elongated grains indicate shear reversion. The latter is also suggested by the rather high dislocation density that remains in the annealed microstructure. In addition to the phase transformation, a slight increase in the grain size after annealing is associated with the development of static recrystallization in work-hardened austenite. The uniform microstructure, with a high dislocation density that evolved by annealing at 600–700 °C,

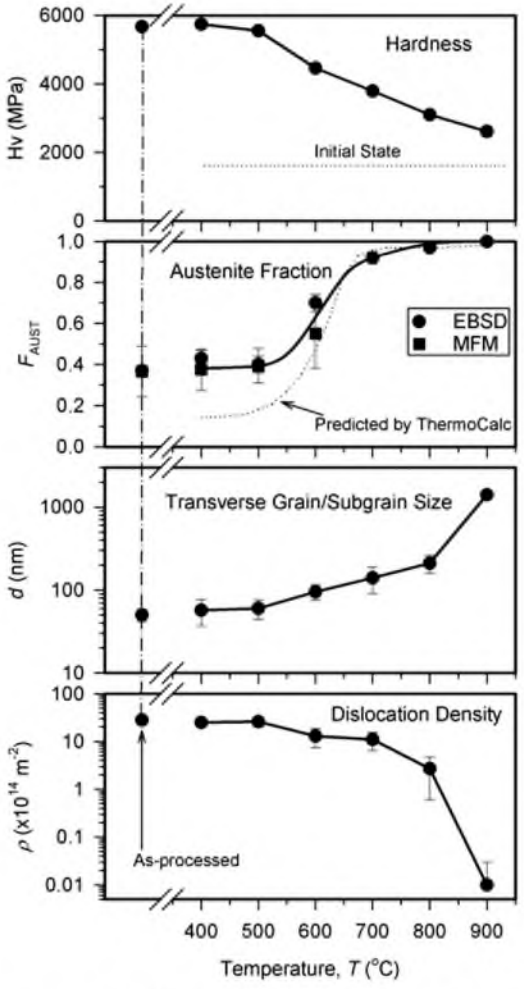

Fig. 12. Effect of annealing temperature on the hardness (Hv), the austenite fraction (F_{AUST}), the grain/subgrain size (d) and the dislocation density (ρ) in an S304H austenitic stainless steel.

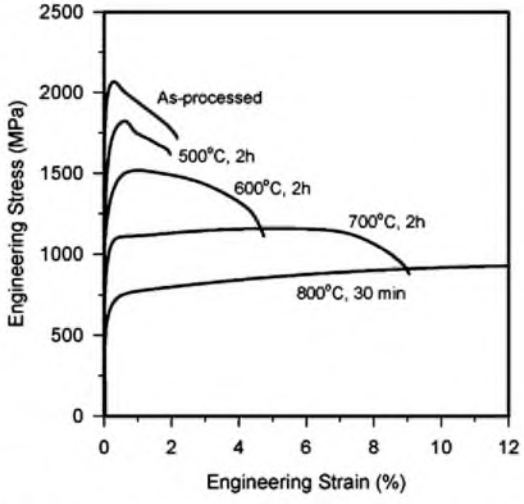

Fig. 13. Engineering σ–ε curves on tensile tests of an S304H austenitic stainless steel processed by cold rolling to a total strain of 4 and then annealed under the indicated conditions.

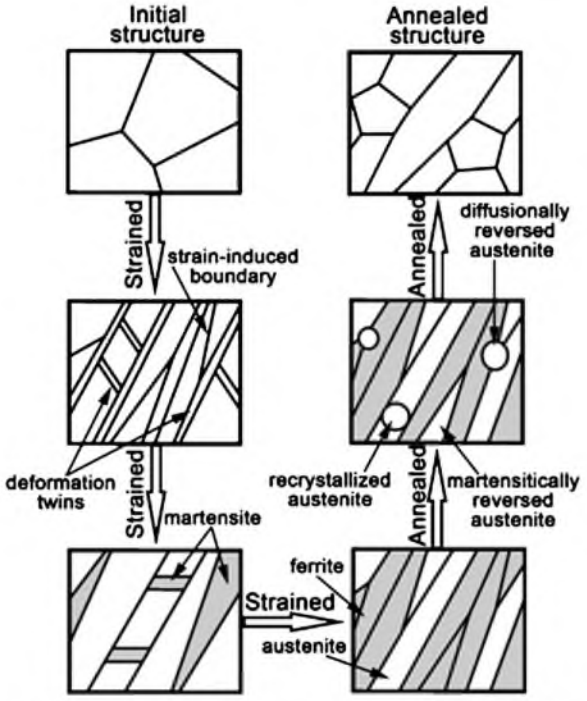

Fig. 14. Schematic representation of the structural changes in an austenitic stainless steel during cold rolling and subsequent annealing.

is indicative of the continuous recrystallization mechanism, which has been observed during the heat treatment of severely deformed stainless steels [53,54]. On the other hand, the diffusion-type reversion mechanism, which provides the formation of essentially equiaxed austenitic grains containing a lower dislocation density in comparison to the surrounding austenite lamellae, is a predecessor of discontinuous recrystallization. At high temperatures of $T \geq 800\,^{\circ}C$, the growth of these grains is driven by both the high density of lattice dislocations in the work-hardened surroundings and the surface boundary energy of the nano/submicrocrystalline structure.

The dual-phase microstructure consisting of austenite and martensite lamellae that develops upon heating severely deformed steel is rather stable against coarsening over long annealing times at temperatures up to 700 °C. The stability of the nano/submicrocrystalline structure during annealing is closely related to the structural characteristics of severely deformed samples. The spacing between sub-boundaries after large-strain cold rolling is very small, and most of the lamellar boundaries are of the high-angle type, which serve as nucleation sites for austenite grains that form during subsequent annealing. The duplex microstructure involving a large fraction of high-angle grain boundaries provides stability to the developed microstructure during annealing, irrespective of a nano-scaled size of the structural elements.

Fig. 15 illustrates the dependence of the offset yield stress on the grain size for Cr–Ni austenitic stainless steels, including the present results along with some other data available in the literature [55–60]. The grain sizes in Fig. 15 cover a wide range, from the conventional micrometer scale down to the nanometer scale. Despite some differences in chemical composition and phase content, all data points in Fig. 15 obey a unique Hall–Petch relationship between the strength and the grain size, i.e., $\sigma_{0.2} = \sigma_0 + K D^{-0.5}$ [61], where $\sigma_0 = 205$ MPa and $K = 395$ MPa $\mu m^{0.5}$. Note that a similar σ_0 value of approximately 200 MPa has been reported for warm to hot-worked ferrous alloys [62]. Fig. 15 clearly shows that the present results provide a link between conventional and nanoscale grains

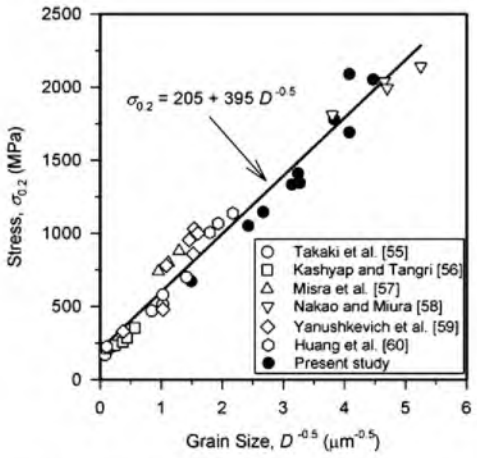

Fig. 15. Relationship between the offset yield strength and the grain size in Cr–Ni stainless steels subjected to different thermo-mechanical treatments.

and unambiguously conform that the Hall–Petch type relationship is valid for Cr–Ni stainless steels in the range of grain sizes down to 50 nm.

5. Conclusions

The deformation and annealed microstructures and the mechanical properties of an S304H-type austenitic stainless steel subjected to large-strain cold rolling and subsequent annealing heat treatment were studied. The main results can be summarized as follows:

1. Cold working is accompanied by multiple deformation twinning and strain-induced martensitic transformation, leading to the evolution of nanocrystalline structure. After cold rolling to a total strain of 4, the deformation microstructure is composed of highly elongated ferrite and austenite grains with a transverse grain/subgrain size of 50 nm; the austenite fraction is approximately 0.35.
2. The developed nanocrystalline structure remains almost unchanged during annealing at temperatures up to 500 °C, while annealing at higher temperatures is accompanied with ferrite–austenite phase transformation by shear and diffusion-reversion mechanisms. The high density of the transformation nucleation sites results in the development of ultrafine-grained microstructure consisting of ultrafine austenite and ferrite grains with a mean grain size below 200 nm after heating to temperatures of 600–700 °C. Remarkable grain growth takes place upon heating to 800 °C, when the austenite fraction increases to about 1.
3. The nanocrystalline steel processed by large-strain cold rolling is characterized by a high tensile strength above 2000 MPa. The offset yield strength decreases to approximately 1000 MPa with an increase in the annealing temperature to 700 °C. The strength of the processed steel depends on the annealing temperature, whereas the holding time does not have a significant effect.
4. The strength of the cold-worked and annealed steel follows a unique Hall–Petch dependence on the grain size, with $\sigma_0 = 205$ MPa and $K = 395$ MPa $\mu m^{0.5}$.
5. Cold rolling to a large total strain followed by annealing at temperatures of 500–700 °C is considered to be an advanced method for processing Ni-Cr stainless steel with a desirable offset yield strength in the range of 1000–2000 MPa.

Acknowledgments

The financial support received from the Ministry of Education and Science, Russia, under grant no. 14.740.11.0333 is gratefully acknowledged. The authors are grateful to the personnel of the Joint Research Centre, Belgorod State University, for their assistance with instrumental analysis.

References

[1] D.G. Morris, in: A.R. Dinesen, M. Eldrup, D. Juul Jensen, S. Linderoth, T.B. Pedersen, N.H. Pryds, S.A. Pedersen, J.A. Wert (Eds.), Science of Metastable and Nanocrystalline Alloys, Riso National Laboratory, Roskilde, Denmark, 2001, pp. 89–94.
[2] Y. Wang, M. Chen, F. Zhou, E. Ma, Nature 419 (2002) 912–914.
[3] R.Z. Valiev, I.V. Alexandrov, Y.T. Zhu, T.C. Lowe, J. Mater. Res. 17 (2002) 5–8.
[4] N. Tsuji, S. Okuno, Y. Koizumi, Y. Minamino, Mater. Trans. 45 (2004) 2272–2281.
[5] Y. Kimura, T. Inoue, F. Yin, K. Tsuzaki, Science 320 (2008) 1057–1060.
[6] F.J. Humphreys, P.B. Prangnell, J.R. Bowen, A. Gholinia, C. Harris, Philos. Trans. R. Soc. London 357 (1999) 1663–1681.
[7] R.Z. Valiev, R.K. Islamgaliev, I.V. Alexandrov, Prog. Mater. Sci. 45 (2000) 103–189.
[8] A. Belyakov, K. Tsuzaki, Y. Kimura, Y. Kimura, Y. Mishima, Mater. Sci. Eng. A 456 (2007) 323–331.
[9] A. Belyakov, K. Tsuzaki, Y. Kimura, ISIJ Int. 48 (2008) 1071–1079.
[10] A. Belyakov, Y. Kimura, Y. Adachi, K. Tsuzaki, Mater. Trans. 45 (2004) 2812–2821.
[11] A. Belyakov, Y. Kimura, K. Tsuzaki, Acta Mater. 54 (2006) 2521–2532.
[12] A. Belyakov, M. Murayama, Y. Sakai, K. Tsuzaki, M. Okubo, M. Eto, T. Kimura, J. Electron. Mater. 35 (2006) 2000–2008.
[13] S.V. Zherebtsov, G.S. Dyakonov, A.A. Salem, S.P. Malysheva, G.A. Salishchev, S.L. Semiatin, Mater. Sci. Eng. A 528 (2011) 3474–3479.
[14] R.D.K. Misra, Z. Zhang, P.K.C. Venkatasurya, M.C. Somani, L.P. Karjalainen, Mater. Sci. Eng. A 527 (2010) 7779–7792.
[15] A. Belyakov, K. Tsuzaki, R. Kaibyshev, Mater. Sci. Forum 667–669 (2011) 553–558.
[16] G.B. Olson, M. Cohen, Metall. Trans. A 6A (1975) 791–795.
[17] S. Allain, J.-P. Chateau, O. Bouaziz, S. Migot, N. Guelton, Mater. Sci. Eng. A 387–389 (2004) 158–162.
[18] L. Bracke, K. Verbeken, L. Kestens, J. Penning, Acta Mater. 57 (2009) 1512–1524.
[19] S. Curtze, V.-T. Kuokkala, Acta Mater. 58 (2010) 5129–5141.
[20] I. Ucok, T. Ando, N.J. Grant, Mater. Sci. Eng. A 133 (1991) 284–287.
[21] M. Eskandari, A. Najafizadeh, A. Kermanpur, Mater. Sci. Eng. A 519 (2009) 46–50.
[22] B.R. Kumar, S. Sharma, B. Mahato, Mater. Sci. Eng. A 528 (2011) 2209–2216.
[23] A. Rezaee, A. Kermanpur, A. Najafizadeh, M. Moallemi, Mater. Sci. Eng. A 528 (2011) 5025–5029.
[24] K. Tomimura, S. Takaki, S. Tanimoto, Y. Tokunaga, ISIJ Int. 31 (1991) 721–727.
[25] K. Tomimura, S. Takaki, Y. Tokunaga, ISIJ Int. 31 (1991) 1431–1437.
[26] D.L. Johannsen, A. Kyrolainen, P.J. Ferreira, Metall. Mater. Trans. A 37A (2006) 2325–2338.
[27] S. Rajasekhara, P.J. Ferreira, L.P. Karajalainen, A. Kyrolainen, Metall. Mater. Trans. A 38A (2007) 1202–1210.
[28] M.C. Somani, P. Juntunen, L.P. Karjalainen, R.D.K. Misra, A. Kyrolainen, Metall. Mater. Trans. A 40A (2009) 729–744.
[29] M. Eskandari, A. Kermanpur, A. Najafizadeh, Metall. Mater. Trans. A 40A (2009) 2241–2249.
[30] F. Forouzan, A. Najafizadeh, A. Kermanpur, A. Hedayati, R. Surkialiabad, Mater. Sci. Eng. A 527 (2010) 7334–7339.
[31] N. Nakada, H. Ito, Y. Matsuoka, T. Tsuchiyama, S. Takaki, Acta Mater. 58 (2010) 895–903.
[32] A. Das, S. Sivaprasad, P.C. Chakraborti, S. Tarafder, Mater. Sci. Eng. A 528 (2011) 7909–7914.
[33] K.H. Lo, C.H. Shek, J.K.L. Lai, Mater. Sci. Eng. R 65 (2009) 39–104.
[34] K.-H. Mayer, F. Masuyama, in: F. Abe, T.-U. Kern, R. Viswanathan (Eds.), Creep-Resistance Steels, Woodhead Publishing Limited, Cambridge, England, 2008, pp. 15–77.
[35] R.E. Schramm, R.P. Reed, Metall. Trans. A 6A (1975) 1345–1351.
[36] G.B. Olson, M. Cohen, Metall. Trans. A 7A (1976) 1897–1904.
[37] R. Kaibyshev, K. Shipilova, F. Musin, Y. Motohashi, Mater. Sci. Eng. A 396 (2005) 341–351.
[38] D.B. Williams, C.D. Carter, Transmission Electron Microscopy, Plenum Press, New York, 1996, pp. 289–298.
[39] J. Gil Sevillano, P. van Houtte, E. Aernoudt, Prog. Mat. Sci. 25 (1981) 69–412.
[40] A. Belyakov, T. Sakai, H. Miura, K. Tsuzaki, Philos. Mag. A 81 (2001) 2629–2643.
[41] Q. Liu, X. Huang, D.J. Lloyd, N. Hansen, Acta Mater. 50 (2002) 3789–3802.
[42] C. Kobayashi, T. Sakai, A. Belyakov, H. Miura, Philos. Mag. Lett. 87 (2007) 751–766.
[43] T.-H. Lee, C.-S. Oh, S.-J. Kim, S. Takaki, Acta Mater. 55 (2007) 3649–3662.
[44] T.-H. Lee, E. Shin, C.-S. Oh, H.-Y. Ha, S.-J. Kim, Acta Mater. 58 (2010) 3173–3186.
[45] S.J. Hales, T.R. McNelley, H.J. McQueen, Metall. Trans. A 22A (1991) 1037–1047.
[46] F.J. Humphreys, M. Hatherly, Recrystallization and Related Annealing Phenomena, Pergamon Press, Oxford, UK, 1996.

[47] K. Tsuzaki, X. Huang, T. Maki, Acta Mater. 44 (1996) 4491–4499.
[48] T.R. McNelley, M.E. McMahon, Metall. Mater. Trans. A 28A (1997) 1879–1887.
[49] Y. He, S. Godet, J.J. Jonas, Appl. Crystall. 39 (2006) 72–81.
[50] H. Landheer, S.E. Offerman, R.H. Petrov, L.A.I. Kestens, Mater. Sci. Forum 558–559 (2007) 1413–1418.
[51] J.W. Christian, S. Mahajan, Prog. Mater. Sci. 39 (1995) 1–157.
[52] S. Zherebtsov, G. Salishchev, S.L. Semiatin, Philos. Mag. Lett. 90 (2010) 903–914.
[53] A. Belyakov, K. Tsuzaki, Y. Kimura, Y. Mishima, J. Mater. Res. 22 (2007) 3042–3051.
[54] A. Belyakov, T. Sakai, H. Miura, R. Kaibyshev, K. Tsuzaki, Acta Mater. 50 (2002) 1547–1557.
[55] S. Takaki, S. Tanimoto, K. Tomimura, Y. Tokunaga, Tetsu-to-Hagane 74 (1988) 118–124.
[56] B.P. Kashyap, K. Tangri, Acta Metall. Mater. 43 (1995) 3971–3981.
[57] R.D.K. Misra, S. Nayak, S.A. Mali, J.S. Shah, M.C. Somani, L.P. Karjalainen, Metall. Mater. Trans. A 41A (2010) 3–12.
[58] Y. Nakao, H. Miura, Mater. Sci. Eng. A 528 (2010) 1310–1317.
[59] Z. Yanushkevich, A. Mogucheva, M. Tikhonova, A. Belyakov, R. Kaibyshev, Mater. Charact. 62 (2011) 432–437.
[60] C.X. Huang, G. Yang, C. Wang, Z.F. Zhang, S.D. Wu, Metall. Mater. Trans. A 42A (2011) 2061–2071.
[61] E.O. Hall, Proc. Phys. Soc. B 64 (1951) 747–753.
[62] C.M. Young, O.D. Sherby, J. Iron Steel Inst. 211 (1973) 640–647.